Dosimetric measurements of electron and photon yields from solid targets irradiated with 30 fs pulses from a 14 TW laser

M. Schnürer,[1] R. Nolte,[2] A. Rousse,[3] G. Grillon,[3] G. Cheriaux,[3] M. P. Kalachnikov,[4] P. V. Nickles,[4] and W. Sandner[4,5]
[1]*Photonics Institute, Vienna University of Technology, Gusshausstrasse 27/359, A-1040 Vienna, Austria*
[2]*Physikalisch-Technische Bundesanstalt, P.O. Box 3345, D-38023 Braunschweig, Germany*
[3]*Laboratoire d'Optique Appliquée, ENSTA–Centre de l'Yvette, F-91120 Palaiseau, France*
[4]*Max-Born-Institut, Max-Born-Straße 2A, D-12489 Berlin, Germany*
[5]*Physics Department, Berlin Technical University, Berlin, Germany*
(Received 30 August 1999)

A 14 TW Ti:Sa laser furnishing pulses with a duration of 30 fs (full width at half maximum) at a repetition rate of 10 Hz was used to expose solid targets to intensities of up to $3\times10^{18}\,\mathrm{W/cm^2}$. Dosimetric techniques were employed to study the total x-ray yield, the spectral and angular distribution of the x-ray photons and the energy distribution of high-energy electrons injected into the solid target and emitted into the vacuum. Scans of laser pulse energy and duration were carried out to study the dependence of the x-ray generation efficiency on these parameters. The radiation transport processes in the target were modeled using the Monte Carlo method. The results of these calculations were used to interpret the measurement results and to critically discuss the applicability of dosimetric methods to the investigation of photon and electron emission from laser-produced plasmas.

PACS number(s): 52.25.Nr, 52.40.Nk, 52.50.−b, 87.53.Bn

I. INTRODUCTION

Progress in the development of Ti:Sa lasers and of the chirped pulse amplification (CPA) technique made it possible to construct compact solid-state laser drivers at the TW power level. Today these laser systems provide intensities which up to now could be realized only with large-scale laser systems. They can be used for the development of compact sources of hard x rays by focusing ultrashort laser pulses on solid targets. The outstanding properties of these sources, namely, their energy distribution, brilliance, source size, and pulse duration, have to be determined and optimized. Numerous investigations into the production of hard x-ray photons with energies above 10 keV from solid-state targets irradiated with short laser pulses have been carried out in the last few years [1–12]. The laser pulse duration ranged from several ps down to less than 100 fs. To provide a better understanding of the interaction of short laser pulses with plasmas and solids, more experimental data, in particular results of absolute measurements of the hard x-ray yield, are required to validate theoretical models.

When high-intensity laser pulses interact with solid targets electrons are accelerated to energies in the MeV range. These high-energy electrons produce bremsstrahlung during their slowing-down in the solid target material. For the efficient generation of high-energy electrons not only the electric field at the target surface but also the production of a plasma layer is of importance [13]. It is well known that collisionless absorption mechanisms (e.g., resonance absorption) and plasma instability processes (e.g., Raman decay instability) can enhance the electric field strength by some orders of magnitude and therefore play an important role in the energy conversion process. The importance of plasma formation for these phenomena shows up in bremsstrahlung emission from plasmas produced with short-pulse lasers at intensitity levels above 10^{14}–$10^{15}\,\mathrm{W/cm^2}$ [14] or in the bright $\frac{3}{2}\omega$, 2ω, and 3ω emission which accompanies the emission of hard x rays [15,16]. Plasma production and plasma density gradients determining these processes sensitively depend on the contrast of the laser pulse. As a consequence the interplay of pulse duration, temporal pulse shape and pulse intensity during plasma production as well as the emission of hard x rays have to be studied. The CPA technique allows the laser pulse duration and energy to be scanned easily. This facilitates the search for optimum conditions for the production of hard x rays.

In this work an extension of previous investigations [17] to a different range of laser power and pulse duration is reported. A 14 TW Ti:Sa laser system with a pulse duration of 30 fs and a repetition frequency of 10 Hz was employed for studies of hard x-ray and hot-electron production during laser-solid interaction. Special emphasis was put on the scaling of hard x-ray emission with pulse duration and energy and on the measurement of the conversion efficiency. In addition to measurements of the x-ray emission, the energy distribution of the high-energy electrons was directly investigated by dosimetric methods.

II. EXPERIMENTAL SETUP

The experiments were performed with the Ti:Sa CPA laser system [18] at the Laboratoire d'Optique Appliquée (LOA), which consists of a 20 fs master oscillator and three multipass amplification stages. Pulses with energies up to 440 mJ and a minimum duration of 30 fs [full width at half maximum (FWHM)] were used to irradiate solid Ta and Al targets at an angle of incidence of 45° in *p*-polarization geometry. The time-averaged power of the laser pulses amounted to 14 TW. The Ta target had thicknesses of 0.5 and 0.025 mm; the thickness of the Al target was 2 mm. No special surface conditioning was applied to the target mate-

rial. The laser-amplifier-chain was operated at a repetition frequency of 10 Hz. Due to the limitations of the target positioning system, a fresh target spot was exposed at every tenth shot, blocking the pulse propagation in between by an electronic shutter system.

The pulse energy was determined behind the off-axis parabolic mirror to include all losses in the focusing optics. The pulse duration was measured at full pulse energy with a second-order correlator and the pulse shape with a third-order correlator. The pulse shape showed a pedestal with an intensity of $10^{-5}I_{\max}$ which was reached 1 ps before the intensity reaches its maximal value $I_{\max}$. The intensity then grew up to $4\times10^{-3}I_{\max}$ within 800 fs and finally increased to the maximum value within 200 fs. The nominal pulse duration (FWHM) of the laser pulse was 30 fs. A CCD camera was used to measure the diameter of the focal spot at reduced laser intensity and with beam focusing under vacuum conditions. From the measured energy content within the spot having a diameter of 20 μm an energy fluence rate of 3×10^{18} W/cm^2 is obtained at full laser power.

The emission of ionizing radiation from the focal spot was characterized using dosimetric techniques which allow the dead-time problems inherent in pulse-counting techniques to be avoided. Different kinds of passive detection systems based on thermoluminescence (TL) detectors and an ionization chamber (manufacturer: RFT-Elektronik) were employed.

A few-channel x-ray spectrometer consisting of a stack of filters and 100 mg/cm^2 LiF:Mg,Ti TL detectors [17,19] served to measure the spectral energy fluence Ψ_E of the x rays in the energy range from 15 to 700 keV. The spectrometer was mounted at a distance of 15 cm from the target spot with the viewing axis oriented normal to the target surface. Figures 1(a) and 1(b) show schemetical drawings of the experimental set-up and of the few-channel spectrometer, respectively. With the exception of the entrance window, the spectrometer was shielded against background radiation by 5 mm Pb and 5 mm Cu. The Cu shield serves to absorb fluorescence radiation induced in the surrounding Pb shield. The outer shielding of the spectrometer effectively absorbs photon radiation with energies up to about 300 keV. For higher energies this is not sufficient for complete suppression of background from scattered photons or photons produced by electrons impinging on the walls of the vacuum chamber. However, a simulation of the experiment using the EGS4 Monte Carlo code system [20,21] showed that at the location of the few-channel spectrometer the spectral fluence of background photons was always less than 5% of the spectral fluence of bremsstrahlung photons produced in the target. Hence no significant deterioration of the measured dose distributions is to be expected.

In Fig. 2(a) the response (D/Φ) of the spectrometer, i.e., the dose reading D per unit fluence Φ of monoenergetic photons, is shown as a function of photon energy $E_{\rm ph}$ for the detector layers of the spectrometer. The response matrix was calculated with the EGS4 Monte Carlo code system. Compared to our earlier work, the energy resolution of the few-channel spectrometer was improved by additional filters and by optimizing their thickness. The SAND algorithm [22] was used to unfold the detector readings. The unfolding procedure was restricted to the energy range from 15 to 700 keV.

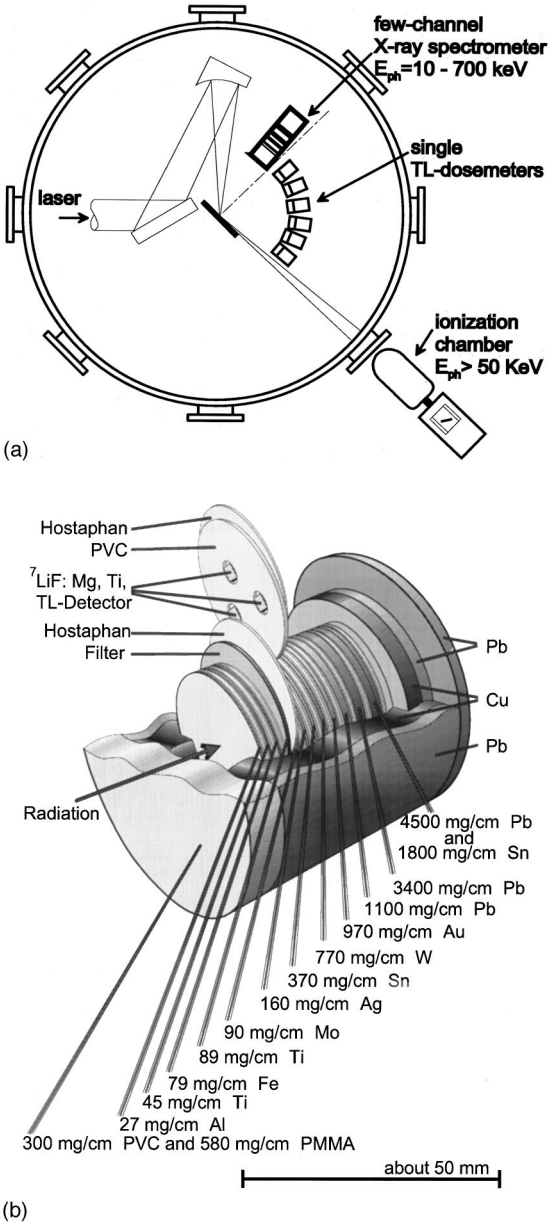

FIG. 1. (a) Schematical drawing of the experimental setup. The diameter of the vacuum chamber was 100 cm. The aspherical mirror had a focusing length of 30 cm. (b) Schematical drawing of the few-channel x-ray spectrometer with the outer shielding against scattered radiation.

Above this energy range the response of the spectrometer depends only marginally on photon energy, thus impairing unfolding of the high-energy part of the spectral distribution. Hence a self-consistent correction was applied to the measured dose values to allow for the contribution from photons with energies above 700 keV. This correction was based on an extrapolation of the spectral energy fluence Ψ_E to high photon energies assuming an asymptotic dependence $\Psi_E \propto \exp(-E/kT)$. This dependence is expected for thick-target bremsstrahlung produced by electrons with a Maxwellian energy distribution with temperature kT.

In laser-solid interaction experiments a mixed photon-electron radiation field is produced. For this reason the sensitivity of the photon few-channel spectrometer to electrons is of importance. In Fig. 2(b) the response (D/Φ) caused by

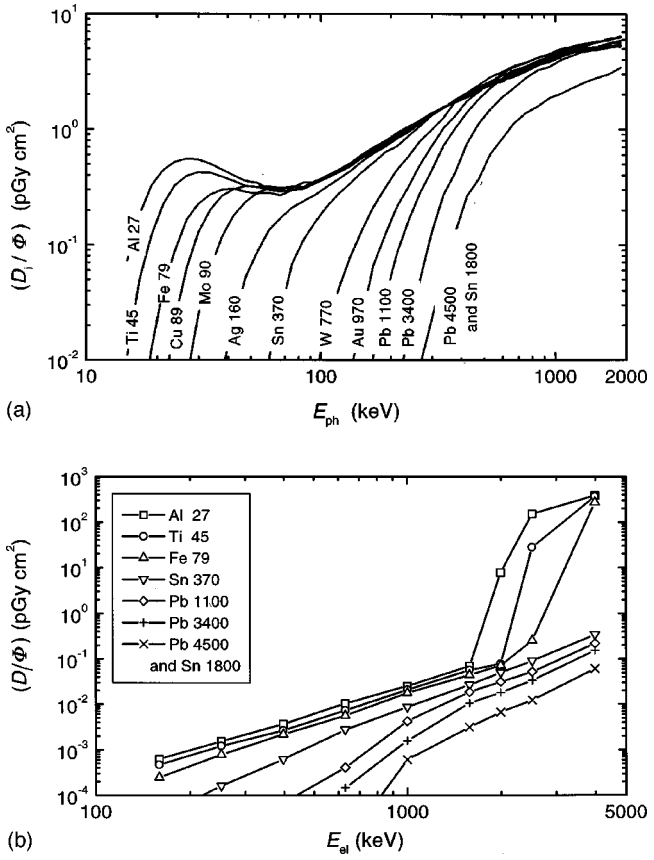

FIG. 2. (a) Response of the few-channel x-ray spectrometer to monoenergetic photons. The areal mass of the filters is denoted in units of mg/cm^2. In front of the spectrometer an electron absorber made of 300 mg/cm^2 PVC and 580 mg/cm^2 PMMA is mounted. (b) Response of the few-channel x-ray spectrometer to monoenergetic electrons. Only selected detector layers are shown.

electron radiation is shown for selected detector layers. For electron energies below 1.5 MeV this sensitivity results from the production of bremsstrahlung in the thick PMMA+PVC filter which prevents electrons from reaching the detector layers. In this case the response to electrons is less than 10% of the photon response. For electrons with energies above 1.5 MeV the electron absorber becomes transparent and the electrons cause a direct dose contribution in the first detector layers. This leads to a considerable increase in the electron sensitivity. Hence a correction had to be applied to the measured dose values to avoid overestimation of the photon component of the radiation field.

The few-channel photon spectrometer essentially relies on the energy dependence of the depth-dose distribution for photon radiation. The same principle can also be employed to construct a few-channel spectrometer for electrons which makes use of the energy dependence of the electron range in LiF. As a first attempt a stack of 100 mg/cm^2 LiF:Mg,Ti TL detectors was employed to investigate the spectral distribution of energetic electrons emitted into the vacuum during the interaction of laser pulses with the target. The twelve TL detectors were embedded in a PMMA cylinder surrounded by an outer shielding similar to that of the few-channel photon spectrometer. On the front side facing the target, the detector stack was covered with an 8 mg/cm^2 Al foil to prevent UV light from causing spurious dose readings. The stack was mounted at the same distance and in the same direction to the target as for the photon few-channel spectrometer. With the set-up outlined above the instrument covered the energy range from 200 keV to 1.5 MeV. With an appropiate unfolding algorithm it should be possible to recover the spectral electron fluence from the measured depth-dose distribution if the fluence of electrons above 1.5 MeV is negligible and the response matrix of the instrument can be calculated with sufficient accuracy. At the present stage of development, however, an experimental verification of this response matrix is not available. For this reason the instrument was only used to check the consistency of measured depth-dose distributions with those calculated for electron energy distributions derived from the analysis of the photon spectra.

Single TL dosemeters equipped with additional filters of 2 mm Pb were placed inside the target chamber to map the angular distribution of the x-ray emission. The range of viewing angles relative to the normal on the target surface extended from 0° to 80°. Additional dosemeters were placed on the outside of the target chamber 1 m in diameter with steel wall 7 mm thick. These dosemeters were designed for the measurement of photon dose-equivalent H_x and served to monitor the potential exposure of the personnel to ionizing radiation. For 3500 shots with a total laser pulse energy of 1.47 kJ, a photon dose-equivalent H_x of 0.45 mSv was measured which is of the same order of magnitude as the annual effective dose due to ambient radiation.

III. RESULTS AND DISCUSSION

For the investigation of the hard x-ray spectrum 3500 laser pulses with a pulse energy of 420 mJ and a pulse duration of 30 fs (FWHM) were focused on the 0.5 mm Ta target. Under these conditions even the most heavily shielded rear detectors of the few-channel spectrometer showed dose readings well above the background caused by ambient radiation. As mentioned above, the few-channel spectrometer has a residual sensitivity to high-energy electrons. Because the electron fluence exceeds the x-ray photon fluence in the radiation fields produced during the interaction of the laser-solid interaction it is important to understand the effect of the electron component on the interpretation of the measurement results. This is why it was attempted to separate the photon and electron contribution to the dose readings of the few-channel spectrometer by a simulation of the experiment.

The EGS4 Monte Carlo code system was used to calculate the x-ray and electron radiation field produced during the slowing-down of the high-energy electrons in a solid Ta target. The electron energy distribution was parameterized by superpositions of two Maxwellians. The relative contributions of the two Maxwellians were adjusted so as to reproduce the unfolded x-ray spectra. The standard EGS4 code system was slightly modified by replacing of the default bremsstrahlung cross section with a data set which is more accurate in the low-energy region [23]. The production of *K*-photons after electron impact ionization was also included [24]. EGS4 models the transport of electrons and photons in nonionized matter [20]. Hence effects caused by the presence of a plasma layer or by the influence of time-dependent electromagnetic fields on the motion of the electrons are not

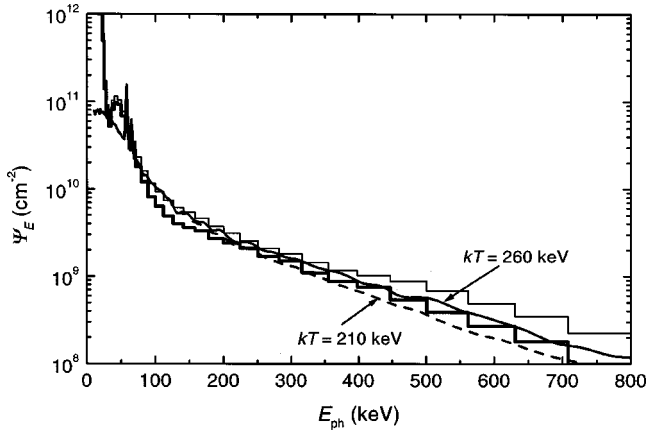

FIG. 3. Spectral energy fluence of x-ray photons produced with 30 fs (FWHM) laser pulses focused on a 0.5 mm Ta target. For this measurement 3500 laser pulses with a total energy of 1.47 kJ were accumulated. The thin and the thick histogram denote the experimental spectrum obtained without and with a correction for the dose contribution from high-energy electrons incident on the spectrometer front face. The solid and the dashed smooth lines represent photon spectra calculated with EGS4 for the electron energy distributions shown in Fig. 3.

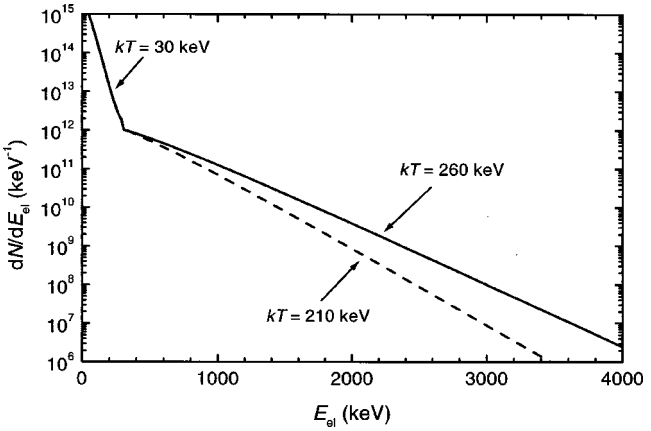

FIG. 4. Electron energy distribution used for the calculation of the bremsstrahlung spectrum represented by the solid and the dashed smooth lines in Fig. 2. The angular distribution was assumed to be isotropic.

included in the present simulation.

The electron spectra resulting from the comparison of simulations and experiment were used to determine the relative contribution of electron radiation to the detector readings. This contribution sensitively depends on the angular characteristic of the production of high-energy electrons by the laser pulse. Calculations showed that the relative contribution of high-energy electrons to the dose readings would be negligible if the electrons were predominantly accelerated into the target because in this case only backscattered low-energy electrons would enter the spectrometer. However, if the angular distribution was more or less isotropic, the high-energy electrons would cause a sizable effect. For reasons discussed below, the latter hypothesis regarding the angular distribution was adopted for the present analysis. The iterative correction performed to allow for the contribution from high-energy electrons was smaller than 30% of the dose reading for all detectors. In future experiments this correction can be avoided by placing a cleaning magnet in front of the few-channel spectrometer.

The results of the analysis are shown in Fig. 3. The thin histogram shows the spectral energy fluence Ψ_E unfolded from the measured dose values without electron correction. The thick histogram indicates the spectral energy fluence unfolded after correction of the measured dose values for the contribution of high-energy electrons. The smooth line shows the spectral energy fluence calculated with EGS4 for the electron energy distributions depicted in Fig. 4. These electron energy distributions were also used to calculate the correction to the dose readings. The two distributions differ in the temperature of the high-energy Maxwellian which were 210 and 260 keV, respectively. The temperature of the low-energy Maxwellian was 30 keV in both cases. As mentioned above, the angular distribution was assumed to be isotropic. The photon spectrum calculated using the electron distribution with the 260 keV Maxwellian (solid smooth line) gives a reasonable fit to experimental data, whereas the electron distribution with the 210 keV Maxwellian (dashed smooth line) results in a photon spectrum which is below the measured data. This demonstrates the sensitivity of the photon spectrum to the electron energy distribution.

The fit of unfolded and calculated x-ray spectra was restricted to photon energies above 50 keV. The strong rise of the unfolded spectral energy fluence below 50 keV therefore is not covered by the calculated spectra. An additional 6 keV Maxwellian component of the electron energy distribution would be required to reproduce the unfolded spectra in this energy region. However, due to the small bremsstrahlung yield of low-energy electrons, the total energy contained in this 6 keV component would exceed the total energy of the laser pulses by more than one order of magnitude. Hence it has to be concluded that the strong rise of the spectral energy fluence at photon energies below 50 keV is an artifact caused by electrons with energies above 1.5 MeV. These electrons can reach the first TL detector layers in the filter stack and cause another dose contribution in addition to that due to photons [see Fig. 2(b)]. In this case the response (D/Φ) to electrons is higher than that to photons by up to two orders of magnitude. A few electrons with energies above 1.5 MeV will therefore be sufficient to produce the strong rise in the unfolded photon spectra at low energies if the respective dose contribution is interpreted as caused by photons. Obviously the self-consistent correction for the contribution of electrons to the detector readings is not capable of taking these very energetic electrons in account.

From the electron energy distribution shown in Fig. 4 the efficiency of the generation of hot electrons by the laser pulse can be obtained. The energy E_h contained in the 30 keV and the 260 keV Maxwellians will amount to 0.77 kJ if a cutoff at an electron energy of 10 keV is applied. The total energy E_L of the 3500 laser pulses was 1.47 kJ. Hence the conversion efficiency E_h/E_L of laser energy to energy of hot electrons is 0.52. This is within the range of results from former experiments [3].

The x-ray spectra provide only information about the distribution of the hot electrons directed into the target. For an investigation of the emission of hot electrons in the opposite direction, i.e., into the vacuum, direct detection of the high-energy electrons is required. This was accomplished with the

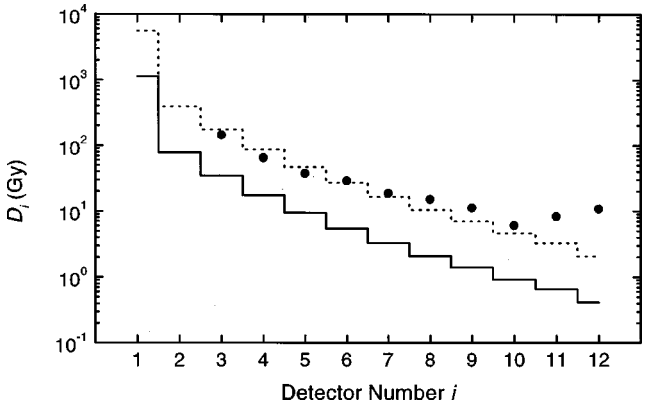

FIG. 5. Depth-dose distribution caused by high-energy electrons in a stack of 12 LiF:Mg,Ti TL detectors with an areal mass of 100 mg/cm^2 each. The detector stack was surrounded by PMMA. The parameters of the laser pulses were the same as for the photon measurements. The experimental data are represented by the dots. The solid histogram is a depth dose distribution calculated for the electron energy distribution shown in Fig. 3; the dashed curve is the same spectrum multiplied by a factor of 5.

stack of TL detectors. Fig. 5 shows the experimental depth-dose distribution. This measurement was carried out with the 2 mm Al target. The parameters of laser pulses were the same as for the photon measurements. For measured dose values above 1 Gy the experimental data were corrected for the supralinearity effect [25]. In Fig. 5 the first two detector readings are lacking because the dose values were above the dynamic range of the TL reader system. Hence the TL detector stack is sensitive only to the electron energy distribution above about 250 keV. The depth-dose curve shows high dose values even for the deepest lying detectors. This indicates that the energy distribution of the hot electrons has a component above 1.5 MeV which cannot be completely stopped in the detector stack. As discussed above these electrons could effect the strong rise in the unfolded photon spectrum at low energies.

In Fig. 5 a depth-dose distribution curve calculated with EGS4 is shown in comparison with the measured distribution. Because no x-ray measurements were carried out for the Al target, the electron energy distribution obtained from the x-ray measurements carried out with the 0.5 mm Ta target (see Fig. 4) was used for the calculation. This procedure is reasonable because the energy distribution of the primary high-energy electrons should not depend very sensitively on the nuclear charge Z of the target. The calculated depth-dose distribution has the same slope as the experimental one. This is an indication that at high energies the shape of the electron spectrum derived from the photon measurements is consistent with the depth-dose distribution caused by the hot electrons emitted into the vacuum. However, the measured depth-dose distribution is higher than the calculated one by about a factor of 5. This cannot be explained by the sensitivity of the TL detector stack to photon radiation. Calculations showed that even for the x-ray spectrum indicated in Fig. 3 by the smooth thin line the depth-dose distribution in the TL detector stack is much smaller than the measured one. Hence it has to be concluded that the high-energy part of the electron spectrum was higher for the Al target than for the Ta target by about a factor of 5. Our finding shows that at least the high-energy part of the hot-electron spectrum produced in laser-plasma interactions at the present power level is not unidirectional, i.e., that an efficient acceleration mechanismen exists that ejects hot electrons also into the vacuum. This also provides some support for the approach taken for the calculation of the electron correction applied to the dose readings of the few-channel photon spectrometer.

The Monte Carlo calculations of the x-ray spectra shown in Fig. 3 (smooth lines) were made on the assumption that the motion of the electrons inside the non-ionized part of the target is not influenced by electromagnetic fields. It has, however, been argued by Bell *et al.* [26] that this hypothesis may be questionable because due to the finite conductivity of the target material large electrostatic fields could be generated to preserve charge neutrality. These fields can act as a transport barrier which prevents high-energy electrons from penetrating very deep into the nonionized target material. For laser intensities of 10^{18} W/cm^2 a penetration depth of only 10 μm is predicted by this model. If this transport barrier was effective, it should also affect the measured bremsstrahlung spectrum. In this case the spectral energy fluence should be independent of the target thickness for targets thicker than the penetration depth. The conclusions by Bell *et al.* are supported by experiments with layered targets [27]. In these experiments the penetration depth inferred from the production of K_α photons was inconsistent with the expected range of the high-energy electrons in the target material.

It was tried to verify the existence of such a transport barrier by comparing the high-energy x-ray yield for two targets of different thicknesses. The spectrum obtained for the target 0.5 mm thick is shown in Fig. 3. In addition, the x-ray spectrum produced with a 0.025 mm Ta target was measured for the same laser pulse energy and the same focusing conditions as for the 0.5 mm Ta target. The thickness of the 0.5 mm and the 0.025 mm target corresponds to the range of 1100 keV and 120 keV electrons, respectively. The 0.5 mm target can therefore be regarded as a ''thick'' target, whereas the 0.025 mm target is ''thin.'' With the correction for the contribution of high-energy electrons discussed above, the spectral energy fluence of the x rays from the 0.025 mm target was consistent with that from the 0.5 mm target in the energy range from 100 to 700 keV, i.e., the experimental spectra agree with spectra calculated for the same electron energy distribution (see Fig. 4) but different target thicknesses. This could be interpreted as an indication that a transport barrier was not effective in the present experiments. However, due to the smaller x-ray yield of the thin target, the relative importance of the correction for electron radiation became so dominant for this target (up to 70%) that the conclusions derived from the comparison of the x-ray spectra for the two targets were very depended on the assumptions underlying the calculations of these corrections. Hence no unambigous information on the existence of a transport barrier could be derived from these experimental data.

The relative angular distribution of the x-ray emission in front of the target is shown in Fig. 6. These measurements were carried out with TL dosemeters equipped with additional filters made of 2 mm Pb. With these filters the cutoff energies for x rays was around 300 keV. The distributions do not show any prominent nonuniform features for the two

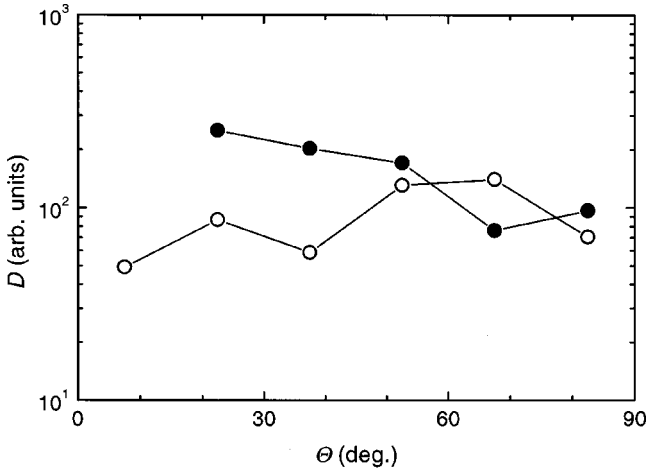

FIG. 6. Angular emission characteristic measured with TL dosemeters equipped with additional filters of 2 mm Pb filter (closed circle: 0.5 mm Ta target, open circle: 0.025 mm Ta target). The reading M of the dosemeters is shown as a function of the angle Θ relative to the normal on the target surface.

targets, which can be explained by the dominating influence of multiple scattering on the electron trajectories in the target. This result is in line with our findings at lower laser intensities [17].

The scaling of the x-ray emission with laser parameters was investigated with an ionization chamber. This instrument was placed outside the target chamber behind a 20 mm Al window which results in a cutoff energy around 50 keV. The viewing angle was almost parallel to the target surface. For this investigation the laser was operated as described above at an effective target shot repetition rate of 1 Hz. Scans of the laser pulse energy E_L and pulse duration τ_L were carried out. In Figs. 7 and 8 the dependence of the reading M of the ionization chamber on these two quantities is shown.

For the interpretation of the measurements it is important to know the relation between the total x-ray energy E_X and the reading M. This relation is determined by the absorption

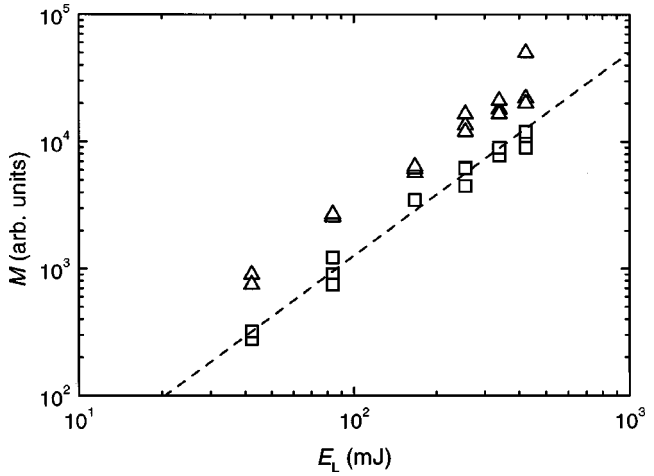

FIG. 7. Reading M of the ionization chamber as a function of laser energy on target (triangles: pulse duration 150 fs; squares: pulse duration 30 fs). The dotted line indicates a scaling law $I_X \propto E_L^{1.5}$.

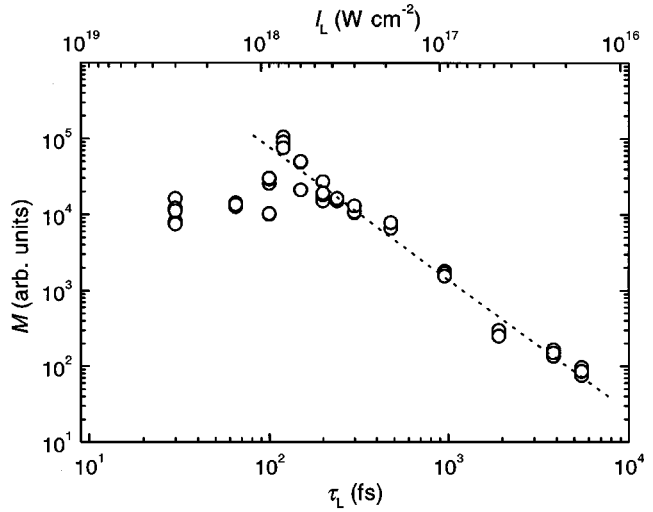

FIG. 8. Reading M of the ionization chamber as a function of laser pulse duration τ_L for a laser pulse energy E_L of 0.4 J. The corresponding laser intensity $I_L = E_L/(\pi r^2 \tau_L)$ is indicated at the upper horizontal axis. The radius r of the focal spot was 10 μm. The dotted line shows a scaling law $I_X \propto I_L^{1.7}$.

of the x-rays in the Al window and the dependence of the x-ray spectrum on the shape of the electron energy distribution. For a Maxwellian electron distribution with temperature kT the relation between E_X and the reading M of an ionization chamber calibrated for the measurement of air kerma K_a is approximately given by

$$M \approx \frac{E_X}{4\pi r^2} \int (\mu_{en}/\rho)_{air} \frac{1}{kT} \exp(-E/kT) \exp(-\mu_{A1} d) dE. \tag{1}$$

Here $(\mu_{\mathrm{en}}/\rho)_{\mathrm{air}}$ denotes the energy absorption coefficient of air divided by the density and μ_{Al} the total attenuation coefficient of Al, r is the distance between the center of the ionization chamber and the focal spot, and d denotes the thickness of the Al window. It is assumed that the x rays are

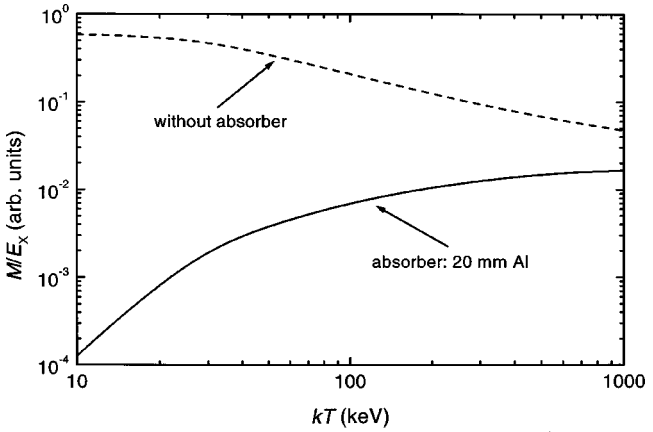

FIG. 9. Dependence of the ratio of the reading M of the ionization chamber and the total x-ray energy E_X on the temperature kT of a Maxwellian electron energy distribution. Data for a filtration of the x-ray spectrum by 20 mm of Al (solid curve) and without any filtration (dashed curve) are shown. The scaling of M with E_L was calculated according to Eq. (1).

emitted isotropically and that the self-absorption in the target can be neglected. Figure 9 shows that the reading M is not proportional to E_L if the electron temperature varies as is to be expected for a scan of either E_L or τ_L. The reason for this is the energy dependence of the absorption coefficients. Figure 9 demonstrates that the total x-ray energy E_X cannot be determined from a dose measurement without some information about the x-ray spectrum.

It is therefore difficult to compare the results shown in Figs. 7 and 8 with other experiments unless the experimental conditions are the same. In Fig. 7 the result of a variation of the laser pulse energy E_L is shown. The pulse durations during these scans were 30 and 150 fs. The reading M followed a scaling law $M \propto E_L^{1.6}$. This scaling law agrees with that found by Kmetec *et al.* [1] for the scaling of E_X with E_L. A fit with a model proposed by Chichkov *et al.* [14] is also possible, but neither the accuracy of the data nor the scan range allows a decision as to whether this fit provides an improved approximation of the measured data. The scaling exponent obtained in this work is significantly smaller than that of earlier investigations at lower laser intensities and greater pulse durations [3,6]. This shows that more detailed measurements covering several orders of magnitude and suitable modeling are required to clarify the somewhat puzzling situation.

In Fig. 8 the scaling of E_X with the laser pulse duration τ_L at a constant laser pulse energy $E_L = 0.4\,\mathrm{J}$ is shown. The most striking feature of Fig. 8 is the saturation of the x-ray emission for pulse durations smaller than 120 fs. It could be interpreted as a signature for plasma confinement due to the ponderomotive pressure. However, in view of the caveats discussed above, this may be somewhat premature because the ratio of the reading M of the ionization chamber and the total x-ray energy E_X may depend on the shape of the x-ray spectrum, i.e., on the electron temperature kT, which may change when the pulse duration is varied.

IV. SUMMARY

Earlier investigations of hard x-ray production from short pulse laser solid target interaction were extended up to a laser irradiation power of 14 TW using pulses as short as 30 fs and intensities up to $3 \times 10^{18}\,\mathrm{W/cm^2}$. The conversion efficiency of laser energy to energy of hot electrons was found to be around 50%. There is evidence for an efficient acceleration mechanism ejecting high-energy electrons from the target surface into the vacuum. A possible saturation of the x-ray production efficiency for laser pulse durations shorter than 120 fs remains to be confirmed by improved experimental techniques.

ACKNOWLEDGMENTS

This work was funded in part by the Commission of the European Communities within the framework of the ''Access to Large Facilities'' Programme. We are grateful to P. Ambrosi for his support for and interest in this work as well as for stimulating discussions.

[1] J. D. Kmetec, C. L. Gordon III, J. J. Macklin, B. E. Lemoff, G. S. Brown, and S. E. Harris, Phys. Rev. Lett. **68**, 1527 (1992).
[2] K. Herrlin, G. Svahn, C. Olsson, H. Petterson, C. Tillmann, A. Persson, C. G. Wahlström, and S. Svanberg, Radiology **189**, 65 (1993).
[3] M. Schnürer, M. P. Kalashnikov, P. V. Nickles, Th. Schlegel, W. Sandner, N. Demchenko, R. Nolte, and P. Ambrosi, Phys. Plasmas **2**, 3106 (1995).
[4] C. L. Gordon III, G. Y. Yin, B. E. Lemoff, Perry M. Bell, and C. P. J. Barty, Opt. Lett. **20**, 1056 (1995).
[5] C. Tillmann, A. Persson, C.-G. Wahlström, S. Svanberg, and K. Herrlin, Appl. Phys. A: Solids Surf. **61**, 333 (1995).
[6] M. Schnürer, P. V. Nickles, M. P. Kalachnikov, W. Sandner, R. Nolte, P. Ambrosi, J. L. Miquel, A. Dulieu, and A. Jolas, J. Appl. Phys. **80**, 5604 (1996).
[7] H. Schillinger, Ch. Ziener, R. Sauerbrey, and H. Langhoff (unpublished).
[8] M. Yoshida, Y. Fujimoto, Y. Hironaka, K. G. Nakamura, Kenichi Kondo, M. Ohtani, H. Tsunemi, Appl. Phys. Lett. **73**, 2393 (1998).
[9] C. Gahn, G. Pretzler, A. Saemann, G. D. Tsakiris, K. J. Witte, D. Gassmann, T. Schatz, U. Schramm, P. Thirolf, and D. Habs, Appl. Phys. Lett. **73**, 3662 (1998).
[10] P. V. Nickles, P. V. Kalachnikov, P. J. Warwick, K. A. Janulewicz, W. Sandner, U. Janke, D. Hilscher, M. Schnürer, R. Nolte, and A. Rousse, Quantum Electron. **26**, 165 (1999).
[11] M. D. Perry, J. A. Sefcik, T. Cowan, S. Hatchett, A. Hunt, M. Moran, D. Pennington, R. Snavely, and S. C. Wilks, Rev. Sci. Instrum. **70**, 265 (1999).
[12] J. Yu, Z. Jiang, and J. C. Kieffer, and A. Krol, Phys. Plasmas **6**, 1318 (1999).
[13] W. L. Kruer, *The Physics of Laser Plasma Interactions* (Addison Wesley, New York, 1988), Chap. 13.3 and references therein.
[14] B. N. Chichkov, C. Momma, A. Tünnermann, S. Meyer, T. Menzel, and B. Wellegehausen, Appl. Phys. Lett. **68**, 2804 (1996).
[15] C. Tillmann, Ph.D. thesis, Lund, 1996.
[16] L. A. Gizzi, D. Giuletti, A. Giuletti, P. Audebert, S. Bastiani, J. P. Geindre, and A. Mysorowicz, Phys. Rev. Lett. **76**, 2278 (1996).
[17] M. Schnürer, R. Nolte, T. Schlegel, M. P. Kalachnikov, P. V. Nickles, P. Ambrosi, and W. Sandner, J. Phys. B **30**, 4653 (1997).
[18] J. P. Chambaret, C. Le Blanc, G. Chériaux, P. Curley, G. Darpentigny, P. Rousseau, G. Hamoniaux, A. Antonetti, and F. Salin, Opt. Lett. **21**, 1921 (1996).
[19] R. Nolte, R. Behrens, M. Schnürer, A. Rousse, and P. Ambrosi, Radiat. Prot. Dosim. **84**, 84 (1999).
[20] W. R. Nelson, H. Hirayama, and D. W. O. Rogers, Stanford Linear Accelerator Center, Report No. SLAC-265, 1985 (unpublished).
[21] Y. Namito, National Laboratory for High Energy Physics, Report No. KEK Internal 95-10, 1995 (unpublished).
[22] W. N. McElroy, S. Berg, T. Crocket, and R. G. Hawkins (unpublished).
[23] M. S. Seltzer and M. J. Berger, At. Data Nucl. Data Tables **35**, 345 (1986).

[24] E. Casnati, A. Tartari, and C. Baraldi, J. Phys. B **15**, 155 (1982).

[25] I. Gamboa-deBuen, A. E. Buenfil, C. G. Ruiz, M. Rodríguez-Villafuerte, A. Flores, and M. E. Brandan, Phys. Med. Biol. **43**, 2073 (1998).

[26] A. R. Bell, J. R. Davies, S. Guerin, and H. Ruhl, Plasma Phys. Controlled Fusion **39**, 653 (1997).

[27] T. Feurer, W. Theobald, R. Sauerbrey, I. Uschmann, D. Altenbernd, U. Teubner, P. Gibbon, E. Förster, G. Malka, and J. L. Miquel, Phys. Rev. E **56**, 4608 (1997).